

# Intermittency of plasma edge fluctuation data: Multifractal analysis

B. A. Carreras and V. E. Lynch

*Oak Ridge National Laboratory, Oak Ridge, Tennessee 37831-8070*

D. E. Newman

*Department of Physics, University of Alaska, Fairbanks, Alaska*

R. Balbín

*Asociación Euratom-Ciemat, 28040 Madrid, Spain*

J. Bleuel

*Max-Planck-Institut für Plasmaphysik, Euratom Association, 85740 Garching, Germany*

M. A. Pedrosa

*Asociación Euratom-Ciemat, 28040 Madrid, Spain*

M. Endler

*Max-Planck-Institut für Plasmaphysik, Euratom Association, 85740 Garching, Germany*

B. van Milligen and E. Sánchez

*Asociación Euratom-Ciemat, 28040 Madrid, Spain*

C. Hidalgo

*Oak Ridge National Laboratory, Oak Ridge, Tennessee 37831-8070*

(Received 3 February 2000; accepted 3 April 2000)

Plasma edge fluctuations show a degree of intermittency similar to fluid turbulence. Using fluctuation measurements obtained with Langmuir probe data from two confinement devices, it is shown that plasma fluctuations have a multifractal character over the fluctuation range of scales with intermittency levels comparable to the levels measured in neutral fluid turbulence. In the mesoscale range, that is, for time scales between 10 times the turbulence decorrelation time and plasma confinement time, plasma fluctuations have a structure closer to a monofractal with very low intermittency. © 2000 American Institute of Physics. [S1070-664X(00)00308-6]

## I. INTRODUCTION

Plasma edge fluctuations and induced fluxes measured in several types of confinement devices are self-similar over the mesoscale range of time scales,<sup>1,2</sup> that is, for time scales between 10 times the turbulence decorrelation time and plasma confinement time. The self-similarity parameter varies little from one device to another. At shorter scales, in the fluctuation range, there is not an exact self-similarity of fluctuations and fluxes and the degree of self-similarity breaking is not clearly defined. On the other hand, there is some evidence of intermittency in the fluctuations.<sup>3</sup> This experimental evidence suggests a different scaling of the plasma turbulent fluctuations in different time scale ranges and the possibility of more complicated structures than a single fractal structure.

On the basis of a very simple hypothesis, Kolmogorov deduced the self-similarity of the turbulent velocity fluctuations and the definition of the inertial range.<sup>4</sup> Later on, experiments on neutral fluid turbulence have shown the breakdown of self-similarity for moments of the velocity structure function larger than 3. Multifractal analysis has been a powerful tool in understanding those deviations from self-similarity.<sup>5,6</sup> This evolution in the understanding of fluid turbulence has also led to the development of simple physical models that bring a level of understanding into this complicated field; from the simple eddy mitosis model based on the

Kolmogorov self-similarity to the  $\beta$ ,<sup>7</sup> random  $\beta$ ,<sup>8</sup> and binomial<sup>9</sup> models that introduce the fractal and multifractal concepts.

In understanding plasma turbulence, we often resort to analogy with neutral fluid turbulence as a paradigm to work under. This can be very beneficial for visualizing the turbulence and turbulent transport but if wrong could be very misleading. While we know there are some similarities between fluid and plasma turbulence, for example, the nature of the nonlinear transfer of energy in certain nonlinearities, we also know there are some differences. For example, plasma turbulence has more nonlinearities and more distributed driving and dissipation ranges. Hence, it probably has a very limited or nonexistent inertial range. Therefore, we do not really know if overall this paradigm is valid. To aid validation (or discounting) the neutral fluid picture comparisons of the dynamics must be made at as many levels as possible. To do this one needs a variety of measures of those dynamics.

While it is interesting to pursue the investigation of the similarity structures in plasma turbulence in the hope of gaining some understanding of the basic mechanisms underlying the plasma turbulence, in using the multifractal analysis, we may also hope to clarify comparisons between plasma and fluid turbulence. Because in plasma turbulence there is more than one type of nonlinearities with different spectral cascade directions as well as the  $E \times B$  nonlinearity,

which has a nonlocal character in  $k$ -space, it is not clear that we can attain such goal.

In designing the analysis tools used in the present study, we have followed the Meneveau and Sreenivasan<sup>10</sup> analysis of fluid turbulence. We have also followed some of the methods suggested by Davis *et al.*,<sup>11</sup> who developed the multifractal formalism for more general applications. A first question to resolve in starting the present analysis is what is the relevant measure that we should apply to the plasma fluctuation measurements. The obvious answer lies in the physics that we want to consider. In three-dimensional fluid turbulence, the intermittence is a characteristic property related to the energy dissipation scales. The studies of intermittency are normally focused on the energy dissipation rate, which is defined as

$$\epsilon = \frac{\nu}{2} \left( \frac{\partial u_i}{\partial x_j} + \frac{\partial u_j}{\partial x_i} \right)^2 \quad (1)$$

Here,  $u_i$  is the  $i$  component of the fluctuating velocity and  $\nu$  is the viscosity. Regrettably, there are no direct measurements of energy dissipation rates. To make a reasonable estimate of them, two assumptions are usually made. The first assumption is that the derivative of the velocity parallel to the flow motion has the same information as the full tensor. The second assumption is Taylor's frozen-flow hypothesis, which allows us to take a time derivative instead of a space derivative parallel to the flow. Based on these assumptions, Meneveau and Sreenivasan<sup>10</sup> take as a measure

$$\epsilon \approx \left( \frac{du_1}{dt} \right)^2 \quad (2)$$

From the measurement of one component of the velocity,  $\epsilon$  can be estimated through Eq. (2).

In plasma turbulence, we do not have a starting point like the Kolmogorov invariance properties. We can only make some tentative assumptions about what could be a reasonable measure. For instance, we can consider some measure of the energy such as the density fluctuation squared or the radial velocity squared. We can also consider some quadratic form analogous to Eq. (2) and take the square of the time derivative of the fluctuations. In this analysis, we have tested several measures and we will compare them in what follows.

Another issue in defining those measures is that we cannot use an equivalent assumption to Taylor's frozen-flow hypothesis. For instance, in a wind tunnel, turbulence is generated at the grid position and the flow carries the turbulence across the measuring point. Therefore, measurements taken at different times at a fixed point are equivalent to measurements at different points along the flow. This is not the case of plasma turbulence. In this case, there is generation and damping of turbulence at the same position where measurements are taken. Therefore, it is not possible to clearly separate between poloidal and temporal structures of the turbulence with a single-point measure. Here, we consider both single-point and multipoint measurements to try to sort out between these two types of scales.

For the moment, we can ask whether the measures proposed reflect any intermittency of the plasma turbulence

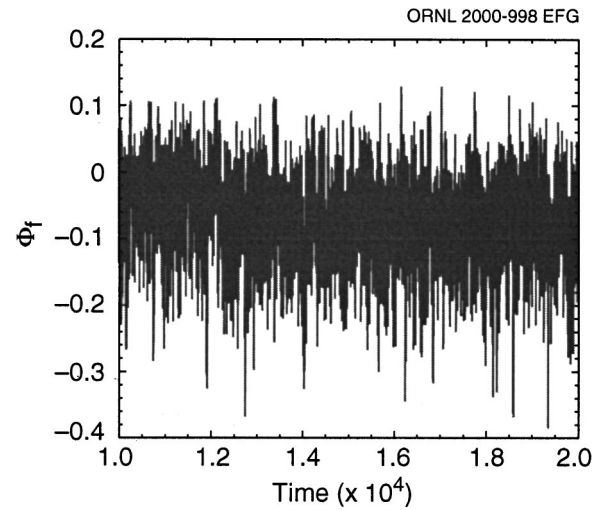


FIG. 1. Density fluctuations inside the shear flow layer for the discharge number 35 427 in the W7-AS stellarator.

fluctuations. The simplest way to find out is by direct visualization. In Fig. 1, we have plotted the floating potential fluctuations as a function of time. This measurement has been done at the plasma edge of the Wendelstein7 Advanced Stellarator (W7-AS).<sup>12</sup> In Sec. III, we discuss the details about these fluctuation measurements. Here, we take the ion saturation current fluctuations as equivalent to density fluctuations and use the floating potential measurements in two poloidal positions to evaluate the fluctuating radial velocity. A simple visual inspection of the signal in Fig. 1 indicates some degree of intermittency. However, when we plot, for the same data, two of the measures discussed previously, the intermittency of the signal is rather more apparent. We have plotted  $(\bar{n} - \langle \bar{n} \rangle)^2 / \langle (\bar{n} - \langle \bar{n} \rangle)^2 \rangle$  in Fig. 2(a) and  $(\bar{V}_r - \langle \bar{V}_r \rangle)^2 / \langle (\bar{V}_r - \langle \bar{V}_r \rangle)^2 \rangle$  in Fig. 2(b) for the same plasma discharge and time as shown in Fig. 1. The angular brackets,  $\langle \rangle$ , indicate time average over the whole time record. These plots in Fig. 2 are quite similar to plots of the normalized energy dissipation rate in fluid turbulence.<sup>10</sup> Therefore, both measures may provide a reasonable description of the intermittence properties of the plasma edge fluctuations. Furthermore, they are an indication that, in plasma edge turbulence, intermittency may be as relevant to the dynamics as it is in fluid turbulence.

The rest of the paper is organized as follows. In Sec. II, we present the analysis methods for single and multipoint fluctuation measurements. The data to be analyzed are described in Sec. III. In Secs. IV and V, we discuss the results of the analysis for the temporal scales. The results for poloidal length scales are described in Sec. VI. Finally, we present our conclusions in Sec. VII.

## II. SCALING OF SINGULAR MEASURES

In the study of plasma edge turbulence, we have basically two types of fluctuation measurements, the ion saturation current and the floating potential. We will assume that the fluctuation component of the first one is equivalent to plasma density fluctuations and the corresponding fluctuation component of the latter is equivalent to the plasma potential fluctuations. From the latter, when we have more than one

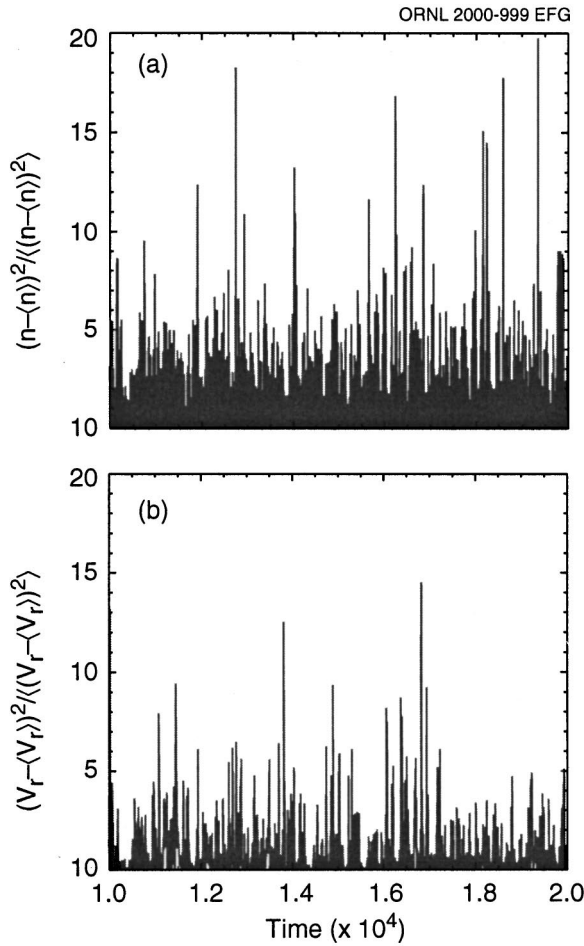


FIG. 2. (a) Square of the density fluctuations normalized to its mean value for the same data set as in Fig. 1. (b) Square of the radial velocity fluctuations normalized to its mean value for the same data set as in Fig. 1.

point measurement, we can derive the velocity fluctuations. Having this information, we can construct the following measures:

$$\epsilon_n \equiv (\bar{n} - \langle \bar{n} \rangle)^2 / \langle (\bar{n} - \langle \bar{n} \rangle)^2 \rangle, \quad (3)$$

$$\epsilon_\Phi \equiv (\bar{\Phi} - \langle \bar{\Phi} \rangle)^2 / \langle (\bar{\Phi} - \langle \bar{\Phi} \rangle)^2 \rangle, \quad (4)$$

$$\epsilon_V \equiv (\bar{V} - \langle \bar{V} \rangle)^2 / \langle (\bar{V} - \langle \bar{V} \rangle)^2 \rangle. \quad (5)$$

We also consider the corresponding measures for the time derivatives of the fluctuations. For instance, in the case of the density fluctuations, we define

$$\epsilon_{\delta n} = [(d\bar{n}/dt) - \langle (d\bar{n}/dt) \rangle]^2 / [\langle (d\bar{n}/dt) - \langle (d\bar{n}/dt) \rangle \rangle]^2. \quad (6)$$

In order to explore the multifractal character of the plasma edge fluctuations, let us now consider the scaling of the previously discussed measures over different scales. In this paper, we investigate separately the scaling over time scales and over poloidal scale lengths. For this reason, we first formulate the analysis for the scaling over times, because this formalism is simpler since it corresponds to a single point measurement. In formulating the analysis approach, we use as an example the case of the density square measure. Similar definitions carry over for other measures.

Given a time series of density fluctuations  $\{n_i; i = 1, 2, \dots, N\}$ , we calculate the measure

$$\epsilon(1, i) = \frac{(n_i - \langle n_i \rangle)^2}{\langle (n_i - \langle n_i \rangle)^2 \rangle}, \quad i = 1, 2, \dots, N, \quad (7)$$

where

$$\langle (n_i - \langle n_i \rangle)^2 \rangle = \frac{1}{N} \sum_{i=1}^N (n_i - \langle n_i \rangle)^2. \quad (8)$$

The next step is to calculate the measure over different time scales. To do so, we average  $\epsilon(1, i)$  over subblocks of data of a length (duration)  $T$  and we define

$$\epsilon(T, i) = \frac{1}{T} \sum_{j=0}^{T-1} \epsilon(1, i+j). \quad (9)$$

The averaging can be done over nonoverlapping blocks or blocks with some degree of overlap. When analyzing simple multifractal structures created by computer modeling, the nonoverlapping blocks worked well. However, in practical applications using experimental data, sometimes the results are too noisy. We found that the results can be improved by allowing overlap between subblocks as a way of increasing the statistics. Using numerical data from multifractal models, we have verified that both techniques produce the same answer.

The next step is to calculate the  $q$  power of the measures over the scale  $T$ ,  $\epsilon(T, i)^q$ , and average over the index  $i$  (number of block considered) to obtain the  $q$ -moment  $\langle \epsilon(T, i)^q \rangle$ .<sup>10</sup> The self-similarity (or self-affinity) of the fluctuations imply that these moments scale as power of the time scale  $T$ ,

$$\langle \epsilon(T, i)^q \rangle \approx \left( \frac{T}{N} \right)^{-K_\tau(q)}. \quad (10)$$

What we are looking for is the exponent  $K_\tau(q)$ . We use the subindex  $\tau$  to indicate that the scaling is over time scales. Note that for a pure self-similarity case (monofractal behavior)  $K_\tau(q)$  scales asymptotically as a linear function of  $q$ . The multifractality is reflected in the nontrivial dependence of  $K_\tau$  on  $q$ . Note that  $q$  does not need to be an integer or even a positive number. Knowing the  $K_\tau$  exponent, we can define

$$C_\tau(q) = \frac{K_\tau(q)}{q-1} \quad (11)$$

and the so-called generalized dimension<sup>13</sup>

$$D_\tau(q) = 1 - C_\tau(q). \quad (12)$$

The parameter  $C_\tau(1)$ , which is calculated as  $C_\tau(1) = dK_\tau(q)/dq|_{q=1}$  to remove the singularity, is called the intermittency parameter. This parameter varies between 0 for a monofractal structure and 1.

The generalized dimension is known under different names for particular values of  $q$ . For instance,  $D_\tau(0)$  is the fractal dimension for support of the measure,  $D_\tau(1)$  is the information dimension, and  $D_\tau(2)$  is the correlation dimension. Again, for a monofractal, all of them have the same value. The variation of  $D_\tau$  with  $q$  gives an indication of what

the degree of multifractality of the system is. Therefore, these functions of  $q$  characterize the multifractal nature of the measure.

To test the analysis code used for the evaluation of the generalized dimension, we have used multifractal models for which the generalized dimensions can be analytically calculated. We use the Mandelbrot approach<sup>6</sup> for a simple generator that is recursively iterated. The simplest generator with structure has three segments (up-down-up). The analytic results are well reproduced by the analysis.

Let us now turn to the determination of the scaling over the poloidal scale length. We use data from multipin probe measurements that will be described in Sec. III and we have generalized the previous analysis technique for the multipoint measurements. This probe measures simultaneously the ion saturation current fluctuation,  $\tilde{I}_s$ , and the floating potential,  $\tilde{\Phi}_f$ , in  $2M$  points which are poloidally separated by a fixed length. From each of these measurements, we have  $M$  data sequences,  $F_j \equiv \{f_i(j); i = 1, 2, \dots, N\}$  with  $j = 1, \dots, M$ . Here,  $f$  is either  $\tilde{I}_s$ ,  $\tilde{\Phi}_f$ , or some other derived quantity. The index  $j$  gives the poloidal position and the index  $i$  is the index of the time sequence. We can now construct a measure generalizing Eq. (3),

$$\epsilon(1, i, j) = \frac{[f_i(j) - \langle f_i(j) \rangle]^2}{\langle [f_i(j) - \langle f_i(j) \rangle]^2 \rangle}, \quad i = 1, \dots, N, \quad j = 1, \dots, M. \tag{13}$$

Here, the angular brackets,  $\langle \rangle$ , indicate averaging over poloidal positions  $j$  and times  $i$ . We can now evaluate the measure  $\epsilon(L, i, j)$  over poloidal separations of length  $L$ ,

$$\epsilon(L, i, j) = \frac{1}{L} \sum_{k=0}^{L-1} \epsilon(1, i, j+k) \tag{14}$$

for each poloidal position  $j$  and each time  $i$ . Then we calculate the corresponding moments of these measures,  $\langle |\epsilon(L, i, j)|^q \rangle$  and perform an average over the indices  $i$  and  $j$  for fixed  $L$ . Again we are looking for the scaling of these moments with  $L$ . If they scale as a power,

$$\langle |\epsilon(L, i, j)|^q \rangle \approx \left( \frac{L}{M} \right)^{-K_l(q)}, \tag{15}$$

we can determine the exponent  $K_l(q)$  and the associated intermittency coefficients,  $C_l(q)$ , and generalized dimension,  $D_l(q)$ , using relations analogous to Eqs. (7) and (8). We use here the subindex  $l$  to indicate that the scaling is over poloidal scale lengths.

For negative values of  $q$ , the moments of the measure are dominated by the smallest events. Of course a serious problem appears if one term in the sum is zero. In this case, the negative moments diverge, as can be seen from Eq. (13). This is a serious problem for the moments of the structure function. It is somewhat unlikely for the moments of the measure to be identically zero because they result from an average over scales. In spite of that, in some situations, there can be very small contributions. Additionally, if the measurements are not a continuous function of time (length), the  $q < 0$  moments reflect the time resolution and the discretization of the measurement. This behavior may cause a misin-

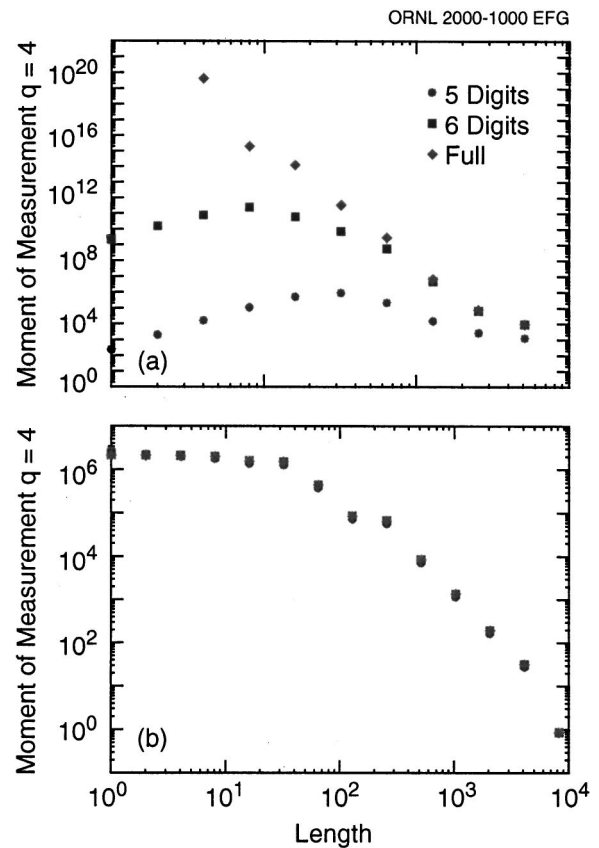


FIG. 3. (a) The  $q = -4$  moments of the square of the time derivative of the density fluctuations for a numerical data set with different numbers of digits resolution. (b) The  $q = 4$  moments of the square of the time derivative of the density fluctuations for the same numerical data set with different numbers of digits resolution.

terpretation of the results. The problem is linked to the number of significant digits in the measurement. This number is limited by the gain used in the measurement and/or digitalization of the data. This has an important impact on the negative moments of the measure. A fair indication of this problem can be obtained by looking at the moments as a function of  $T$ . We have used some numerical data from simple turbulence models (50 000 data points) to test the effect of reducing the number of digits characterizing the elements in a data set. Two tests have been done by multiplying each element in the sequence by  $10^6$  (and  $10^5$  in the second test) making it an integer and dividing it afterward by  $10^6$ . In this way we are limiting the number of digits representing each element. The original data had nine digits. In Fig. 3(a), we have plotted the  $q = -4$  moment of measure for the three cases. Despite the fact that there are no identical cancellations for any of the calculated moments, one can easily see the strong effect that cutting the digits has on the slope of the moment. However, there is no discernible effect for positive values of  $q$  [Fig. 3(b)]. The extreme sensitivity of the negative moments makes it very difficult to imagine that they can be properly evaluated in the case of experimental data. We therefore emphasize the positive  $q$  moments.

To determine the exponents that characterize the multifractal structures, the moments of measure must behave as a power for a reasonable range of values of  $T$  and  $L$ . We take

a range that covers at least a decade to be a “reasonable” range of values of  $T$  and  $L$ . We will discuss in each case the range of scales used in the analysis.

### III. DATA ANALYZED

We have applied this analysis to plasma edge fluctuation data from the Wendelstein 7 Advanced stellarator (W7-AS)<sup>12</sup> and the TJ-I tokamak.<sup>14</sup> In both cases, the data were obtained with Langmuir probe measurements.

In the case of the W7-AS stellarator, we use data from a reciprocating multipin Langmuir probe.<sup>15,16</sup> This probe has 16 pins distributed in the poloidal direction; 8 of them are used to measure the ion saturation current fluctuations,  $\tilde{I}_s$ , and the other 8 to measure the floating potential fluctuations,  $\tilde{\Phi}_f$ . Details of the experimental setup can be found in Ref. 15. The separation between the closest pins measuring the same type of fluctuations is 0.4 cm, except for the two last pins, which are separated 0.8 cm. Therefore, with this probe we can study poloidal scale lengths varying between 0.4 and 3.6 cm. This range is close to a decade of variation for the poloidal scale length. Because the probe is a reciprocating probe, it moves from the scrape-off layer to inside the plasma, covering a distance of about 6 cm in each discharge. The sampling rate is 0.5 MHz and each pin takes 800 000 data points in time. We have analyzed the data sets corresponding to discharges 35 427, 35 432, 35 484, and 35 543. These discharges have been selected because the measurement includes a sizable range (2 cm) of the edge plasma region. For most of the analysis, we break those sets into 40 subsets of 20 000 points. For each of the data sets considered, the probe has only moved about 1.5 mm. Therefore, they can be considered nearly stationary. In this way, we can do a radially dependent analysis of the similarity properties of the fluctuations over both temporal and poloidal scales. We normalized the ion saturation current fluctuation to its time-averaged value in each subject to avoid effects caused by changes in the size of the pins.

For these discharges, the decorrelation time of the fluctuations is about 10  $\mu$ s. The time interval considered for each one of the 40 subsets is 1  $\mu$ s  $\leq T \leq$  10 ms. Therefore, we can study both the fluctuation range ( $T \leq 10 \mu$ s) and the mesoscale range ( $T \geq 100 \mu$ s) of time scales.

The analysis techniques described in Sec. II are applied to the ion saturation current fluctuations,  $\tilde{I}_s$ , which we identify with the density fluctuations, to the floating potential fluctuations,  $\tilde{\Phi}_f$ , and to the poloidal electric field fluctuations, which we define as  $\tilde{E}_\theta = \partial\tilde{\Phi}_f/\partial\theta$ . The latter is obtained from the measured potential by taking differences between measurements done at the closest poloidal positions and neglecting the electron temperature fluctuations. The fluctuating poloidal electric field can also be interpreted as a measure of the fluctuating radial velocity,  $\tilde{V}_r = -\tilde{E}_\theta/B$ .

We have also analyzed a radial scan using a fixed probe through a sequence of nine discharges in the TJ-I tokamak.<sup>14</sup> This sequence goes from discharge number 49 825 to discharge number 49 833. The data have a sampling rate of 1.0 MHz and collect a time sequence of 4000 points. They cover

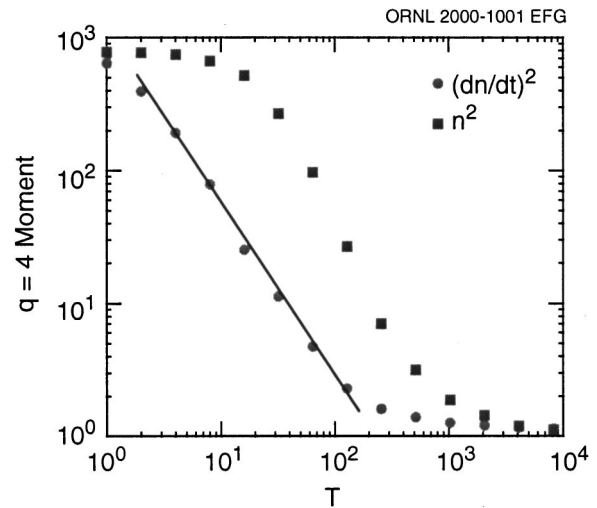


FIG. 4. The  $q=4$  moments of the  $n^2$  and  $(dn/dt)^2$  measures for the data set from discharge 35 427 in W7-AS.

the radial range  $0.91 < r/a_s < 1.08$ . The radial position of the edge plasma shear layer is  $a_s$ . In TJ-I  $a_s \approx 10$  cm, therefore, the radial range considered is less than 2 cm. Because of the short record length, for this data we can only study the fluctuation range of scales. This range is from 1 to about 100  $\mu$ s.

### IV. SCALING WITH TEMPORAL SCALES OF PLASMA EDGE FLUCTUATIONS

In this section, we first consider the results of the analysis taking single-pin measurements in W7-AS. We use this data to find the scaling properties of the fluctuations over different time scale ranges. The first question to resolve is the range of scales over which the moments of the measure scale as a power. At short scales it is easier to define such a range. For large values of  $T$ , the moments of measure tend to saturate at constant value. This is a general result for all measures considered. In the first study of the scaling ranges, we used a record length of 150 000 points. We subtracted a trend in the data caused by the motion of the reciprocating probe. The reason for taking this large sample is to cover as many decades of temporal scales as possible. We have calculated the moments of measure  $\langle \epsilon(T, i)^q \rangle^{1/q}$  for the different measures defined in Sec. II. In plotting the data, we have taken the  $1/q$  power to make it easy to fit them into the same plot. As an illustration of the problems encountered, in Fig. 4, we have plotted the  $q=2$  moments for the  $n^2$  and the  $(dn/dt)^2$  measures. In the latter case, we can see a reasonable range of  $T$  values for which  $\langle \epsilon(T, i)^q \rangle^{1/q}$  is a power function,  $1 < T < 200$ . A power-scaling range is more difficult to find for the  $n^2$  measure. Therefore, we see that the  $(dn/dt)^2$  measure may be more adequate than the  $n^2$  measure to quantify the multifractal properties of plasma fluctuations. We can see also in Fig. 4 that for  $T > 10^3$ , that is for time scales longer than 1 ms, there is a saturation of moments. The same considerations apply to the other measure, such as  $\Phi^2$  and  $V_r^2$ , the derivative square has a clearer power dependence range. However, the discrepancy is more significant for the density square measure. It may be that in the

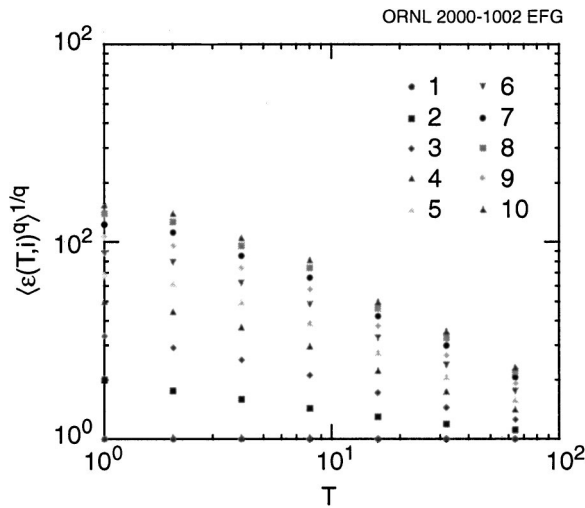


FIG. 5.  $1/q$  power of the moments of the  $(dn/dt)^2$  measure in the fluctuation range of time scales for the same data as in Fig. 5 showing a wide spread of values for the slope.

SOL, plasma density is low and the density square does not represent the energy transfer for the fluctuations.

In Fig. 5, we have plotted the  $1/q$  power of the  $1 > q > 10$  moments of the  $(dn/dt)^2$  measure in the power scaling range. For a monofractal structure, all curves should collapse into a single one. Clearly, there is no collapse of the moments into a single curve. Therefore,  $K_\tau(q)$  is a nontrivial function of  $q$  and the data analyzed has a multifractal character. The same result is obtained for all the other measures.

We can repeat the calculation of the moments for the mesoscale range. In this range, the moments of measure are nearly independent of  $T$  (Fig. 6). Therefore, if we assume that the moments of measure scale as a power in this time scale range, the exponent is practically zero. Since all moments collapse into a single curve, the measure reflects a monofractal structure in this range of scales. Again, the same results are found for all the other measures considered here.

Let us now turn to the determination of the scaling exponents. To do a quantitative determination and avoid any problem with the motion of the probe, we have repeated the

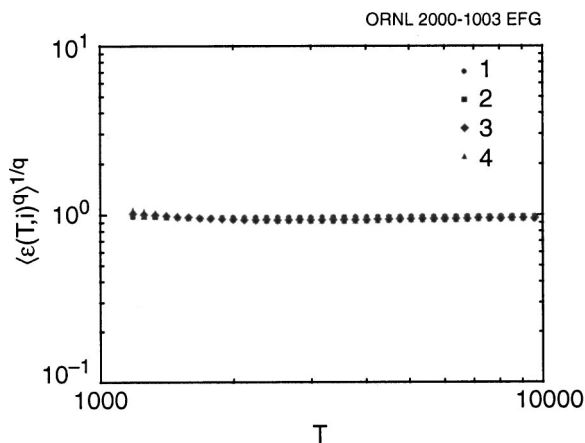


FIG. 6.  $1/q$  power of the moments of the  $(dn/dt)^2$  measure in the mesoscale range of time scales for the same data as in Fig. 5.

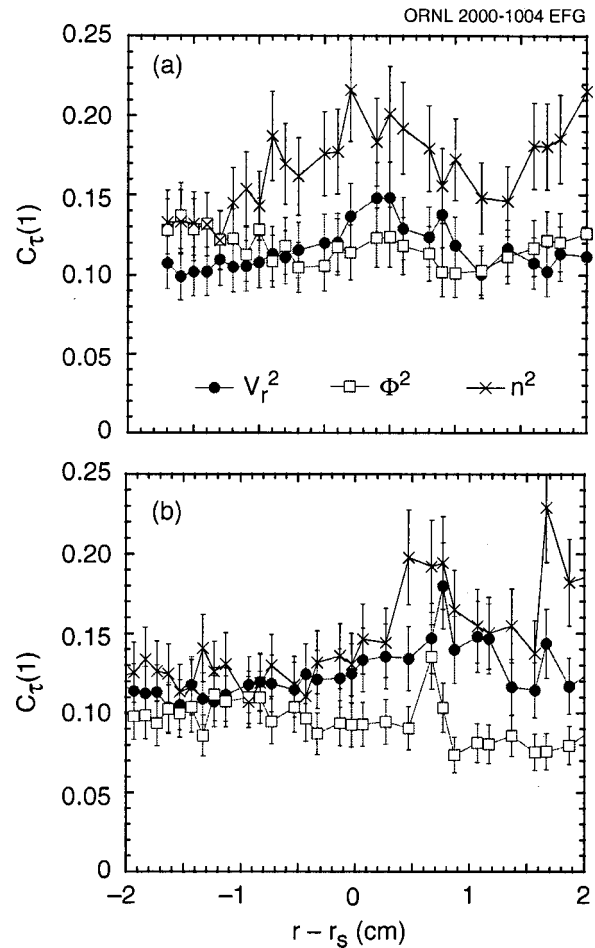


FIG. 7. Intermittency parameter  $C_\tau(1)$  as a function of the radial distance to the zero phase velocity point in the shear layer for the three measures defined by Eqs. (3)–(5) and for discharges: (a) 35427 and (b) 35432 in W7-AS.

analysis by breaking the full data sets into 40 data subsets of 20 000 points. We focus the analysis on the fluctuation and mesoscale ranges separately and we study the radial dependence of the main scaling exponents.

We first consider the fluctuation range. For this range and in Fig. 7, we have plotted the intermittency parameter  $C_\tau(1)$  for the three measures as a function of the radial distance to the zero phase velocity point in the shear layer. The plot is for data from two different discharges. In both discharges, the three measures give very similar values for the intermittency parameter and this value is close to the one obtained in the analysis of fluid turbulence. This parameter is 0 for a monofractal structure and its possible maximum value is 1. It is difficult to make an accurate determination of the errors involved in the calculation of  $C_\tau(1)$ . In Fig. 7 we have only included the statistical errors from fitting the moments of measure with a power function.

Using the time derivative measures, one obtains comparable levels for the intermittency (Fig. 8). These results show that the calculated value for the intermittency is relatively robust.

From this analysis we can evaluate the generalized dimension for the plasma edge turbulence. The calculated val-

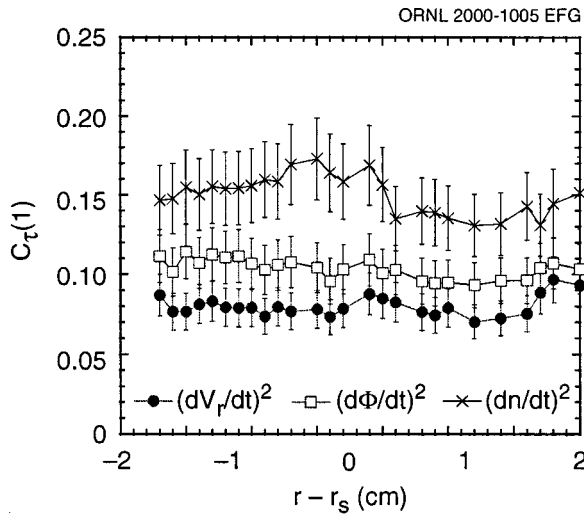


FIG. 8. Intermittency parameter  $C_\tau(1)$  as a function of the radial distance to the zero phase velocity point in the shear layer for the three time derivative measures and for discharge 35 427 in W7-AS.

ues for the generalized dimension can be compared to a fit using the binomial model.<sup>9</sup> This model has been used to interpret cascades in fluid turbulence. The model is a generalization of the eddy mitosis model and it is characterized by a single parameter  $p_1$ . The model assumes that each eddy breaks into two pieces and that each piece receives a fraction  $0.25p_1$  or  $0.25(1-p_1)$  of the flux of kinetic energy. Therefore, the parameter  $p_1$  varies between 0 and 1 and is a measure of the asymmetry in the cascade. If  $p_1=0.5$ , we recover the eddy mitosis model and the monofractality. The process continues iteratively, and at each step the distribution of energy between eddies is a binomial distribution. Therefore, it is possible to calculate analytically the generalized dimension

$$D(q) = \frac{\ln[p_1^q + (1-p_1)^q]}{(1-q)\ln(2)}. \quad (16)$$

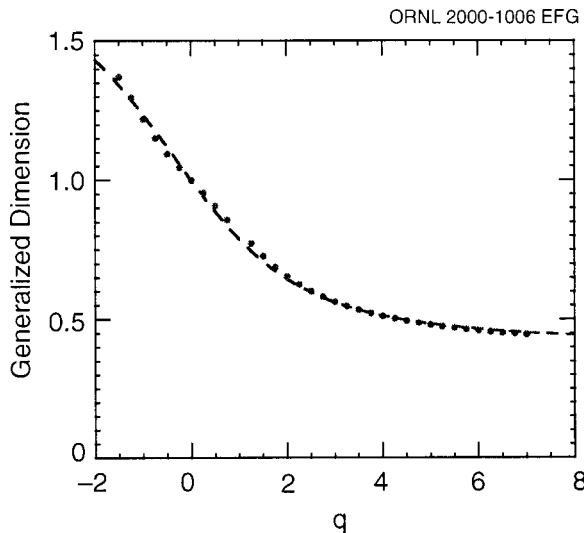


FIG. 9. Generalized dimension as a function of  $q$  together with a fit done with the binomial model.

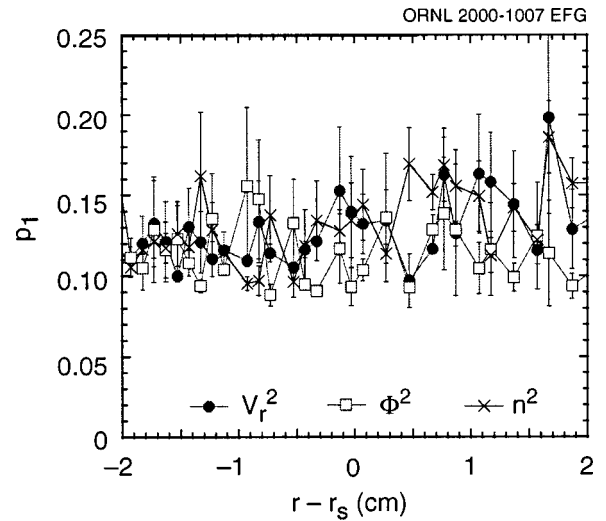


FIG. 10. Values of  $p_1$  obtained by fitting the generalized dimension obtained for the three measures applied to discharge 35 427 in W7-AS.

We have used this expression to fit the calculated generalized dimension at each of the 40 radial positions. In general, this model fits very well the generalized dimension calculated from the fluctuation data. However, since we do not include negative values of  $q$ , the fit is less constrained. An example of the fit for one of the data subsets of discharge 35 427 is given in Fig. 9. The values of  $p_1$  obtained for the three measures applied to this discharge are plotted in Fig. 10. Over the entire range considered, the value of  $p_1$  is somewhat larger than the values reported from fluid turbulence. In that case, the values obtained are close to  $p_1=0.7$ .<sup>10</sup> The mean values of  $p_1$  obtained for the different measures and for the two discharges considered here are given in Table I. The  $\pm$  indicates the standard deviation of the values of  $p_1$  for the 40 radial positions considered. The error in the determination of each of the  $p_1$  values is, in general, larger than the dispersion of values, but difficult to determine. The statistical error from fitting the data with Eq. (16) is on average 0.04, that is, of the same order as the radial dispersion. Within the 0.04 averaged dispersion, all values obtained are consistent. They also seem to be independent of the measure chosen.

The mesoscale range scales correspond to time scales longer than about ten times the decorrelation time of the turbulence, in this particular discharge we take times longer than 0.1 ms. The self-similarity properties for this time scale range have been discussed in Ref. 1. In this time scale range,

TABLE I. Parameter  $p_1$  determined from fitting the generalized dimension associated with temporal scales and poloidal scale lengths from two discharges in W7-AS and for the three measures used in this paper.

Measure	35 427		35 432	
	Temporal	Poloidal	Temporal	Poloidal
$\bar{n}^2$	$0.77 \pm 0.04$	$0.82 \pm 0.02$	$0.77 \pm 0.04$	$0.79 \pm 0.03$
$\Phi^2$	$0.75 \pm 0.03$	$0.73 \pm 0.05$	$0.73 \pm 0.03$	$0.72 \pm 0.05$
$\bar{v}_r^2$	$0.76 \pm 0.04$	$0.81 \pm 0.03$	$0.76 \pm 0.04$	$0.88 \pm 0.03$

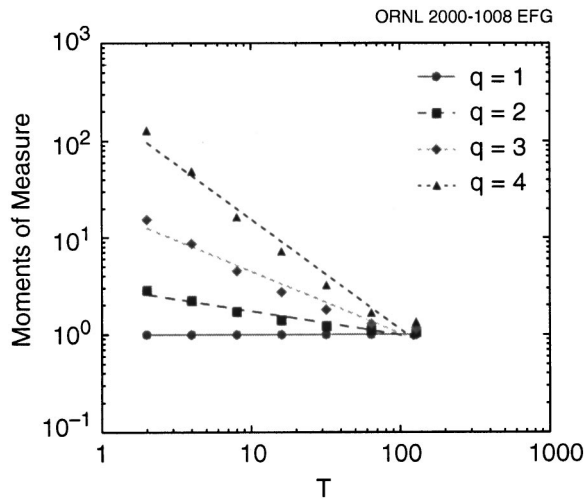


FIG. 11. Moments of square derivative of the density measure for data taken at plasma edge for discharge 49 829 in the TJ-I tokamak.

the moments of measure are practically independent of  $T$  (Fig. 6) and as a consequence the intermittency coefficient is considerably smaller than in the fluctuation range. It is practically zero at all radial positions. The change of the generalized dimension with  $q$  is also found to be very weak in this range. It is difficult to determine whether this variation is real or the fluctuations just obey a monofractal behavior within the error bars of the calculation. This result clearly contrasts with the one obtained for the fluctuation scale range where the structure is clearly multifractal.

To test the generality of the previous results, we have also analyzed plasma edge fluctuation data from the TJ-I tokamak. As discussed before, the record length of the TJ-I data is short, 4000 points. Therefore, we can only study the fluctuation range of scales. This range is from 1 to about 100  $\mu s$ . In Fig. 11, we have plotted the moments of measure,  $\langle \epsilon(T, i)^q \rangle$ . The measure used is the density square measure. The plot is for one of the nine data sets. These moments can be described by a power function over the whole time scale range considered. Therefore, we can determine the intermittency coefficient and generalized dimension for the nine data sets. In Fig. 12, we have plotted the intermittency coefficient  $C_r(1)$  as a function of the radial position. The radial-averaged level of intermittency is  $C_r(1) = 0.17 \pm 0.03$ . This value is comparable to the values obtained for the density fluctuations in W7-AS. The calculated generalized dimension has been fitted using the binomial model.<sup>10</sup> The averaged value of  $p_1$  obtained from those fits is  $0.78 \pm 0.04$ . This value is also close to the ones obtained in the W7-AS analysis (see Table I).

### V. SCALING WITH POLOIDAL LENGTH SCALES OF PLASMA EDGE FLUCTUATIONS

We can only investigate the poloidal length scales for the case of W7-AS measurements, because it is the only available experimental data from a multipin probe measurement. To these data, we have applied the analysis technique described in Sec. III. We have used the measurement of the

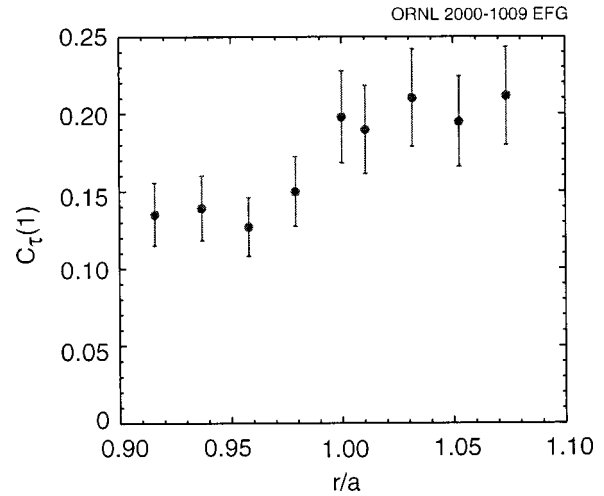


FIG. 12. Intermittency coefficient  $C_r(1)$  as a function of the radial distance to the zero phase velocity point in the shear layer for a sequence of discharges in the TJ-I tokamak.

ion saturation current fluctuations,  $\tilde{I}_s$ , the floating potential fluctuations,  $\tilde{\Phi}_f$ , and the radial velocity fluctuations,  $\tilde{V}_r = -\tilde{E}_\theta/B$ . The latter is evaluated as described in Sec. III. Because of the probe structure, we have only eight length scales over which to test the power scaling. In Fig. 13, we have plotted several moments of measure for the floating potential measurement. In the same figure we also show an example of a power fit to these moments. The moments of measure are consistent with the power dependent fit, but further experiments covering a broader range of scales would be desirable to prove such power scaling. However, those experiments will not be easy because they require either a larger poloidal probe or multiple probe measurements along the poloidal direction. The increase of the poloidal extent of these experiments must be significant to shed any light on

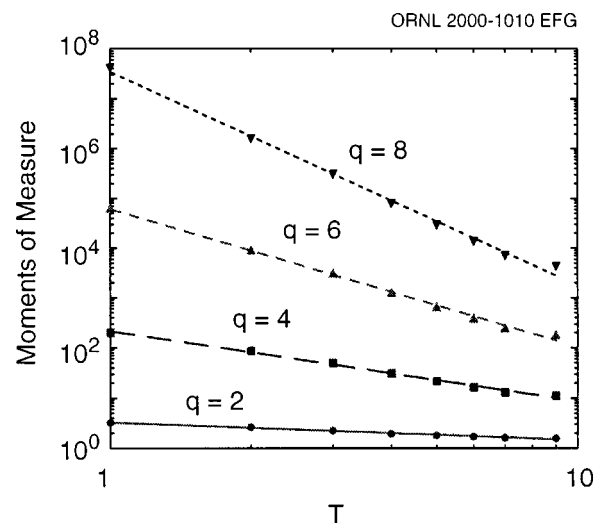


FIG. 13. Several moments of measure for the floating potential measurement as a function of poloidal separation for the discharge 35 427 in W7-AS.

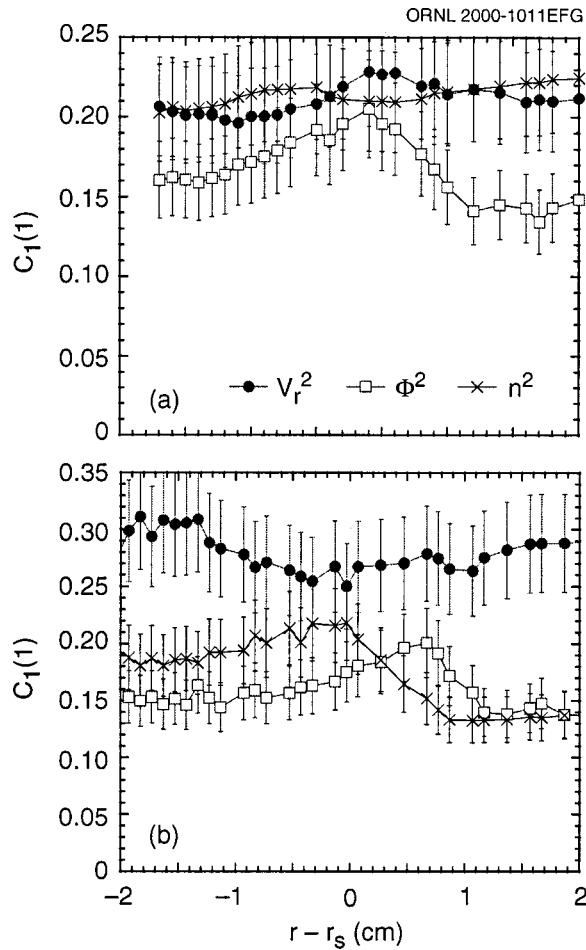


FIG. 14. Intermittency coefficient  $C_I(1)$  as a function of the radial distance to the zero phase velocity point in the shear layer for the three measures defined by Eqs. (3)–(5) and for discharges: (a) 35 427 and (b) 35 432 in W7-AS.

this issue. Here we assume that the power scaling is the right description of the data and we use such fits to determine the scaling exponent.

In Fig. 14, we have plotted the intermittency parameter,  $C_I$ , derived from the poloidal length scaling for  $\tilde{I}_s$ ,  $\tilde{V}_r$ , and  $\tilde{\Phi}_f$ . These plots are analogous to the ones showing the intermittency parameter for the temporal scales (Fig. 7). The intermittency coefficient has been plotted as functions of the radial position. The radially averaged value of both  $C_I(1)$  and  $C_\tau(1)$  for each of the three measures and for the fluctuation range of time scales is given in Table II. The  $\pm$  indicates the standard deviation of the values of these coefficients for the 40 radial positions considered. We can see that  $C_I(1)$  is somewhat larger than  $C_\tau(1)$ . Also the level of intermittency for the floating potential is smaller than the corresponding intermittency for the other fluctuation measurements. This effect has already been noticed in other studies.<sup>3</sup> In Table II, we compare  $C_I(1)$  with  $C_\tau(1)$  for the fluctuation range. The reason is that the poloidal scale lengths considered are of the order and smaller than the poloidal correlation length, which is  $2.1 \pm 0.01$  cm for the W7-AS fluctuation measurements. Therefore, the value for

TABLE II. Intermittency parameter  $C(1)$  associated with temporal scales and poloidal scale lengths from the analysis of two discharges in W7-AS and for the three measures used in this paper.

Measure	35 427		35 432	
	Temporal	Poloidal	Temporal	Poloidal
$\tilde{n}^2$	$0.19 \pm 0.03$	$0.22 \pm 0.01$	$0.16 \pm 0.03$	$0.17 \pm 0.03$
$\tilde{\Phi}^2$	$0.14 \pm 0.03$	$0.17 \pm 0.02$	$0.10 \pm 0.02$	$0.16 \pm 0.02$
$\tilde{V}_r^2$	$0.13 \pm 0.03$	$0.21 \pm 0.01$	$0.13 \pm 0.02$	$0.28 \pm 0.02$

$C_I$  derived here is probably related to the fluctuation range of scale lengths.

## VI. CONCLUSIONS

The results of the analysis of the plasma edge fluctuations in both the W7-AS stellarator and in the TJ-I tokamak show that in the fluctuation range of scales the turbulence has a multifractal structure. This implies that plasma edge turbulence is intermittent at short time and space scales. However, in the mesoscale range, the structure of plasma edge turbulence is monofractal.

The intermittency and the multifractality levels have been determined using three measures which are directly related to the fluctuations measured. The intermittency is characterized by the intermittency coefficient  $C(1)$ . The level of multifractality can be characterized by the value of the parameter  $p_1$  obtained from a fit to the generalized dimension.

For all cases considered, the level of multifractality seems to be the same within the error bars. There is hardly any change in the parameter  $p_1$  with the measure and for the discharges considered. This indicates that the results of the analysis are fairly robust.

The intermittency parameter may change with the edge plasma conditions, but for all the cases, the floating potential fluctuations show a lower level of intermittency than the density and velocity fluctuations. We have not found much difference between the scaling exponents for temporal scales and poloidal scale length, although the level of spatial intermittency is in general higher than the temporal one. This result contrasts with the differences found for the Hurst exponent. The analysis of the structure function indicated that the velocity fluctuations have  $H > 0.5$  for temporal scales and  $H < 0.5$  for poloidal length scales.

The levels of intermittency and multifractality that we found for the plasma edge turbulence measurements are comparable to the levels that have been found for neutral fluid turbulence, with values for  $C(1)$  and  $p_1$  slightly higher for plasma turbulence.

It would be interesting to extend the present analysis to a broader set of measurements and in particular to plasma core fluctuations. To find whether the values for the main parameters used in this analysis have a more universal validity could be important in providing a better understanding of the structure of plasma turbulence.

## ACKNOWLEDGMENTS

This research was sponsored in part by Dirección General de Investigaciones Científicas y Técnicas of Spain under Project No. PB96-0112-C02-02, by Oak Ridge National Laboratory, managed by Lockheed Martin Energy Research Corp. for the U.S. Department of Energy under Contract Nos. DE-AC05-96OR22464, and DE-FG03-99ER54551. We also want to acknowledge the Joint Commission for Scientific and Technological Cooperation between the United States and Spain for their support during the completion of this research

- <sup>1</sup>B. A. Carreras, B. van Milligen, M. A. Pedrosa *et al.*, Phys. Plasmas **5**, 3632 (1998).  
<sup>2</sup>B. A. Carreras, B. van Milligen, C. Hidalgo *et al.*, Phys. Rev. Lett. **83**, 3653 (1999).  
<sup>3</sup>E. Sánchez, C. Hidalgo, D. López-Bruna *et al.*, Phys. Plasmas **7**, 1408 (2000).

- <sup>4</sup>U. Frisch, Turbulence, the Legacy of A. N. Kolmogorov (Cambridge University Press, Cambridge, 1995).  
<sup>5</sup>J. Feder, *Fractals* (Plenum, New York, 1988).  
<sup>6</sup>B. B. Mandelbrot, *Multifractals and 1/f noise* (Springer, New York, 1998).  
<sup>7</sup>U. Frisch, P.-L. Sulem, and M. Nelkin, J. Fluid Mech. **87**, 719 (1978).  
<sup>8</sup>R. Benzi, G. Paladin, G. Parisi *et al.*, J. Phys. A **17**, 3521 (1984).  
<sup>9</sup>C. Meneveau and K. R. Sreenivasan, Phys. Rev. Lett. **59**, 1424 (1987).  
<sup>10</sup>C. Meneveau and K. R. Sreenivasan, J. Fluid Mech. **224**, 429 (1991).  
<sup>11</sup>A. Davis, A. Marshak, W. Wiscombe *et al.*, J. Geophys. Res. B **99**, 8055 (1994).  
<sup>12</sup>H. Renner, the WVII-AS team, the NBI group, the ICF group, and the ECRH group, Plasma Phys. Controlled Fusion **31**, 1579 (1999).  
<sup>13</sup>H. G. E. Hentschel and I. Procaccia, Physica D **8**, 435 (1983).  
<sup>14</sup>I. Garcia-Cortes, M. A. Pedrosa, C. Hidalgo, B. Brañas, T. Estrada, R. Balbin, E. del la Luna, J. Sanchez, and A. P. Navarro, Phys. Fluids B **4**, 4007 (1992).  
<sup>15</sup>M. Endler, H. Niedermeyer, L. Giannone *et al.*, Nucl. Fusion **35**, 1307 (1995).  
<sup>16</sup>J. Bleuel, G. Theimer, M. Endler *et al.*, in Controlled Fusion and Plasma Physics (European Physical Society, Petit. Laney, 1996), Vol. 20C, pp. 727–730.